Efficient Biexciton Emission in Elongated CdSe/ZnS Nanocrystals

ARTICLE *in* NANO LETTERS · SEPTEMBER 2011

Impact Factor: 13.59 · DOI: 10.1021/nl202506c · Source: PubMed

NANO LETTERS

LETTER

pubs.acs.org/NanoLett

Efficient Biexciton Emission in Elongated CdSe/ZnS Nanocrystals

Y. Louyer, L. Biadala, J.-B. Trebbia, M. J. Fernée, Ph. Tamarat, and B. Lounis*

Laboratoire Photonique Numérique et Nanosciences, Université de Bordeaux, Institut d'Optique Graduate School & CNRS, 351 cours de la libération, 33405 Talence, France

ABSTRACT: We use a combination of low-temperature magneto-optical and lifetime spectroscopies to study the band-edge exciton fine structure of highly photostable single CdSe/ZnS nanocrystals (NCs). Neutral NCs displaying multiline emission spectra and multiexponential photoluminescence (PL) decays are studied as a function of temperature and external magnetic fields. Three different fine structure regimes are identified as a function of the NC aspect ratio. In particular, we identify an optically inactive ground exciton state, whose oscillator strength is tuned up under magnetic field coupling to bright exciton states, and attribute it to the zero angular momentum ground exciton state of elongated NCs. We also show evidence for highly efficient biexciton emission in these NCs, with radiative yields approaching unity in some cases.

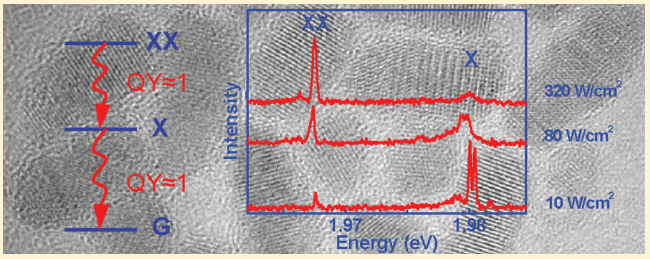

KEYWORDS: CdSe nanocrystals, quantum dots, exciton, biexciton, fine structure, quantum yield

Over the past two decades, significant efforts have been spent on magneto-optical properties of semiconductor nanostructures, motivated by fundamental interests and by potential applications in solid-state spintronics[1] and quantum information processing.[2] Among semiconductor nanostructures, chemically synthesized CdSe nanocrystals (NCs) are particularly attractive due to their bright luminescence, which is size tunable across the visible spectrum and has suitable properties for optoelectronics,[3−6] and biological fluorescent labeling.[7,8] For these applications, it is crucial to understand the interplay between exchange interaction, crystal-field splitting, and quantum confinement leading to the band-edge exciton fine structure.

Because of the hole and electron spins (3/2 and 1/2, respectively), the band edge exciton ($1S_{3/2}-1S_e$) has 8-fold degeneracy that is lifted into five sublevels by the intrinsic electron−hole exchange interaction and by the crystal field of the hexagonal lattice. It is well established on both theoretical and experimental grounds that in spherical or nearly spherical NCs, the exciton ground state is often referred to as the dark exciton since it has a total spin projection on the crystal hexagonal c-axis $J = \pm 2$.[9−11] It is located a few millielectronvolts below the lowest-energy optically active exciton state ($J = \pm 1$). At low temperatures, the photoluminescence (PL) arises from these two thermally mixed excitonic states as evidenced by the study of the PL spectra and decays as a function of temperature and external magnetic fields.[12−16] While intensive experimental and theoretical work has been performed to describe the size dependence of the exciton fine structure in nearly spherical NCs, the shape dependence has received much less attention despite recent advances in NC growth methods that lead to a greater control over shape distribution.[17] Pioneering theoretical and experimental investigations[10,18] have indicated that the shape dependence of NCs can be as important as the size dependence in terms of tuning their electronic and optical properties. Because of the hexagonal structure of CdSe, elongation along the c-axis produces many pronounced changes in the NCs exciton fine structure,[18−20] and consequently in their optical properties. The elucidation of these shape effects remains an experimental challenge which can be addressed by the optical study of individual NCs,[21] where ensemble averaging over shape and size distributions is suppressed.

Shape and size effects also govern the optical response of NCs in the multiexcitonic regime, where potential applications such as optical gain are envisaged.[22] Despite the important role that biexcitons play in the optics of NCs, it has been practically impossible to observe the biexciton recombination line in the PL of CdSe NCs under continuous wave excitation, because of efficient nonradiative Auger recombination.[23] Biexciton signatures in CdSe NCs were observed at room temperature in transient pump−probe transmission[24−26] or transient PL[27−30] experiments. Recently biexciton emission from individual NCs under CW excitation has been reported.[31−33] These studies concern "giant" CdSe/CdS NCs[31,32] or quasi type II CdTe/CdSe NCs[33] where Auger recombination rates are significantly reduced.

In this article, we report magneto-optical and time-resolved spectroscopic investigations of single commercial qdot655 streptavidin conjugates NCs (comprising a core of CdSe capped by a ZnS layer) as a function of temperature. Because of the NCs shape distribution, we find various band-edge exciton fine structures that are consistent with theoretical predictions for elongated NCs. Furthermore, contrarily to what was anticipated for "standard" CdSe-based core shell NCs, we present here the spectral and temporal signatures of highly efficient radiative biexcitonic recombinations for this type of NCs.

Received: July 22, 2011
Revised: September 9, 2011

dx.doi.org/10.1021/nl202506c | *Nano Lett.* XXXX, XXX, 000–000

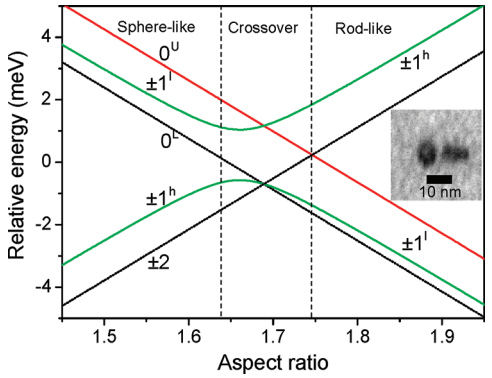

Figure 1. Calculated exciton fine structure of a prolate spheroidal NC of width 7 nm as a function of aspect ratio, using the 8-band model of Efros et al.[10] Three regions are defined as spherelike, crossover, and rodlike. Inset: TEM image of two NCs, illustrating the significant dispersion in NC aspect ratios.

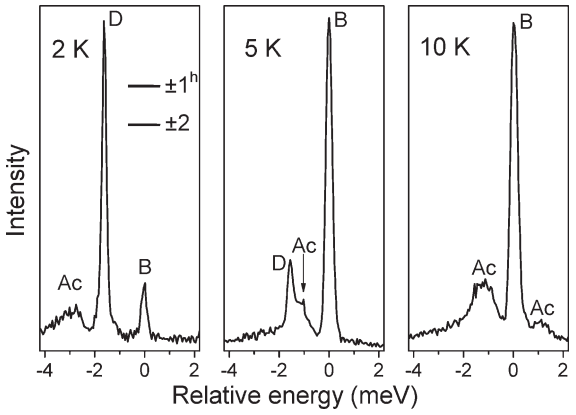

Figure 2. PL spectra of a spherelike single NC recorded at various temperatures. The origin of the energy scale is 2.007 eV. Each spectrum is recorded at an excitation intensity of 100 W/cm^2. The lines labeled B and D are the recombination ZPLs of the bright $|\pm1^h\rangle$ and the dark $|\pm2\rangle$ exciton states, respectively, which are thermally mixed. The labels Ac indicate acoustic phonon sidebands.

For this study, samples are prepared by spin coating clean glass coverslips with a nanomolar solution of NCs (Qdot655 with peak emission at 655 nm at room temperature) in polyvinyl alcohol. A home-built scanning confocal microscope is used to image single NCs excited with the 532 nm line of a cw frequency doubled Nd:YAG laser. It is based on a high numerical aperture objective housed in a magnetic cryostat together with the sample and a piezoscanner. The objective axis is perpendicular to the magnetic field, allowing magneto-optical studies in the Voigt configuration. The emitted photons are filtered from the scattered excitation light by a bandpass filter (60 nm fwhm) and sent to a single photon counting avalanche photodiode and a spectrometer. The PL decay measurements are performed with a conventional time-correlated single photon counting setup, using a pulsed laser source (optical parametric oscillator at 570 nm, 6 ps pulse width, 76 MHz repetition rate) and a pulse picker which reduces the repetition rate. A Hanbury-Brown and Twiss coincidence setup is used to record the PL intensity autocorrelation function of single NCs.

The size and shape characterization of the studied NCs was performed with transmission electron microscopy (see inset of Figure 1). It reveals a significant distribution of NC prolate shapes (width 6 ± 1 nm, length 11 ± 1 nm, aspect ratio 1.8 ± 0.5), in broad accordance with the results of Zhang et al.[34] Theoretical studies predict that the band-edge exciton fine structure strongly depends on the shape[21,35] due to the combined effects of crystal field splitting and quantum confinement. In particular, the highest occupied hole state derives either from the heavy hole band of bulk CdSe (in oblate or spherical NCs) or from its light hole band (in rodlike NCs). Electron−hole exchange interactions split the 4-fold degenerate heavy hole exciton into $|\pm2\rangle$ and $|\pm1^h\rangle$, and the 4-fold degenerate light hole exciton into $|0_L\rangle$, $|\pm1^l\rangle$, and $|0_U\rangle$, which results in two bunches of neighboring levels $\{|0_L\rangle, |\pm1^l\rangle, |0_U\rangle\}$ and $\{|\pm2\rangle, |\pm1^h\rangle\}$, sorted here in ascending order of energy within each bunch. The relative energy position of these bunches depends on the NC shape.[35] The lower energy bunch is $\{|\pm 2\rangle, |\pm1^h\rangle\}$ for a spherical or oblate shape, while it is $\{|0_L\rangle, |\pm1^l\rangle,|0_U\rangle\}$ for a pronounced prolate (or rod) shape along the NC *c*-axis. In Figure 1, we show the theoretical prediction for the spectral fine structure of a CdSe prolate spheroid of width 7 nm using the established 8-band envelope function theory of Efros et al.,[10] plotted here as a function of aspect ratio. We define three regions as spherelike, crossover, and rodlike. This simplified model predicts a crossover region at an aspect ratio ∼1.7 where the strong mixing of $|\pm1^h\rangle$ and $|\pm1^l\rangle$ occurs, in good agreement with atomistic-pseudopotential numerical models.[35] The size and shape of the studied NCs offer the possibility to investigate the transition of the band-edge exciton fine structure between spherelike and rodlike NCs.

Most of the studied NCs display a remarkably stable PL with no blinking and extremely reduced spectral diffusion at 2 K that allows the acquisition of resolution-limited PL spectra over minutes. In Figure 2, we present a typical spectrum of a spherelike single NC and its temperature evolution.[13−15] At 2 K, it displays two sharp zero-phonon lines (ZPLs) that have been attributed to the radiative recombination from the two lowest exciton levels (bright $|\pm1^h\rangle$ and dark $|\pm2\rangle$), as a consequence of a weak spin-flip rate between these two states.[13−15] When raising the temperature from 2 to 10 K, the high-energy ZPL stemming from the bright exciton state dominates the spectrum, providing evidence for thermal mixing between two states of different oscillator strengths. This type of NCs were extensively studied with cw and time-resolved spectroscopy,[12−15] which allowed us to derive the bright and the dark radiative recombination times (∼6 ns and hundreds of ns, respectively) as well as the bright-to-dark spin-flip time (∼1 ns). Magneto-PL studies also led us to characterize magnetic coupling effects between $|\pm2\rangle$ and $|\pm1^h\rangle$ states, as well as their Zeeman splitting.[16]

Markedly different spectroscopic behaviors were also obtained with this NCs sample. Figure 3 exemplifies a second class of NC spectral behavior. In contrast with the spherelike NC of Figure 2, this NC displays a single ZPL at 2 K, labeled β in Figure 3a. When raising the temperature, a second ZPL (labeled γ) appears at higher energy as shown in Figure 3b. The amplitude of γ tends to that of β at temperatures above 10 K, indicating that the emission stems from two optically active states with comparable oscillator strengths. However, application of a magnetic field at 2 K unveils an additional ZPL (named α) which is ∼0.3 meV red shifted with respect to the β line, as displayed in Figure 3c. At fields larger than 2 T, the α line prevails in the PL spectrum, while the Zeeman splitting of the β line into two components is clearly

dx.doi.org/10.1021/nl202506c |*Nano Lett.* XXXX, XXX, 000–000

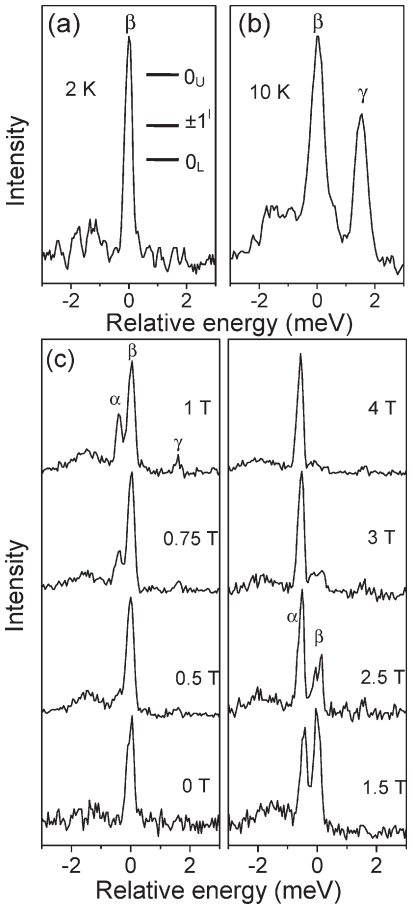

Figure 3. PL Spectra of a single NC at various temperatures (2 K in (a), 10 K in (b)) and under various applied magnetic fields at 2 K (c). The origin of the energy scale is 1.986 eV. Each spectrum is recorded at an excitation intensity of 10 W/cm^2. The lines labeled α, β, and γ are respectively attributed to the recombination ZPLs of the lowest fine structure states $|0_L\rangle$, $|\pm1^l\rangle$ and $|0_U\rangle$ in a rodlike NC.

observed. This evolution suggests that α is the recombination line of an optically forbidden state, whose oscillator strength is drastically enhanced by a field-induced mixing with a neighboring bright exciton state. This mixing is induced by the component of applied magnetic field transverse to the NC c-axis. While the longitudinal component of the field splits the β line into two Zeeman sublevels, indicating that β is the recombination line of a doubly degenerate state, the absence of Zeeman splitting of the α ZPL points to a spin singlet ground excitonic state. Thus, using the magneto-optical properties of the spectra shown in Figure 3c, we can assign these spectra to that emanating from rodlike NCs, where the lines α, β, and γ can be attributed to emissions from the ground dark exciton state $|0_L\rangle$, the bright states $|\pm1^l\rangle$ and $|0_U\rangle$, respectively. Interestingly, the zero-spin ground state of rodlike NCs is a truly dark state from which luminescence is evidenced only under magnetic fields, which contrasts with the case of spherelike NCs where the ground exciton state $|\pm2\rangle$ displays a ZPL radiative recombination at zero external magnetic field.

We also investigated the exciton recombination dynamics of the rodlike NC displayed in Figure 3, by measuring its PL decay at 2 K under various magnetic fields. As shown in Figure 4, the PL decay at zero field is triexponential with characteristic decay

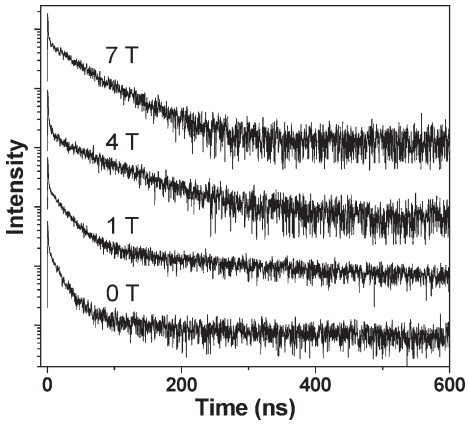

Figure 4. PL decay at 2 K of the NC displayed in Figure 3, for various applied magnetic fields. While the decays were recorded over 800 ns, the displayed time window is limited to 600 ns for a better comparison. The decay is triexponential in zero field with characteristic times ~1, 18, ~220 ns, and becomes biexponential at fields higher than 3 T. The fast decay occurring in the nanosecond range is attributed to the spin relaxation rate of the $|0_U\rangle$ state. The transition from triexponential to biexponential behaviors is a result of magnetic coupling between the lowest exciton states $|0_L\rangle$ and $|\pm1^l\rangle$.

times ~1 (within our resolution scale), 18, and ~220 ns, indicating three relaxation modes. The fast decay occurring in the nanosecond range is attributed to the spin relaxation rate of the $|0_U\rangle$ state, the intermediate decay corresponds to the $|\pm1^l\rangle$ radiative recombination rate, and the longer to the spin relaxation rate from $|\pm1^l\rangle$ to $|0_L\rangle$. As a result of magnetic coupling between $|\pm1^l\rangle$ and $|0_L\rangle$ the longer decay component drastically shortens with increasing fields, until the PL decay becomes biexponential at fields larger than 3 T. The long component of the biexponential decay has a characteristic time of 58 ns at 7 T, approaching the limit of radiative recombination lifetime of $|\pm1^l\rangle$ expected in the strong magnetic coupling regime.

In accordance with theoretical predictions of a strong dependence of the band-edge exciton fine structure on the NC shape, we observed more complex spectroscopic behaviors that likely result from the crossover regime. Figure 5a exemplifies the PL spectrum of a single NC, which displays three ZPLs (labeled β, γ, and δ) in the absence of external magnetic field. When raising the temperature from 2 to 10 K, the high energy ZPL prevails over the two other lines, while the δ ZPL remains twice less intense than the β ZPL. This supports an attribution of the δ and γ recombination lines to exciton states with weakly allowed and allowed radiative relaxations, respectively. As shown in Figure 5d, application of an external magnetic field to the NC at 2 K unveils another ZPL (named α) that is ~0.3 meV red shifted with respect to the β line. At fields larger than 2 T, the α line dominates the PL spectrum. This evolution suggests that α is the recombination ZPL of an optically forbidden exciton state whose oscillator strength is raised by a field-induced coupling to the upper exciton states. A tentative attribution of the α, β, δ, and γ ZPLs to the states $|0_L\rangle$,$|\pm1\rangle$, $|\pm2\rangle$ and $|0_U\rangle$, respectively, is consistent with the theoretical expectations of the band−edge exciton fine structure[21,35] in the crossover regime as shown in Figure 1. This attribution is further strengthened by the observable Zeeman splitting of the β and δ lines, while the lines α and γ do not split under magnetic fields.

An important result obtained with these NCs is the spectroscopic signature of biexciton recombination lines in the

dx.doi.org/10.1021/nl202506c |*Nano Lett.* XXXX, XXX, 000–000

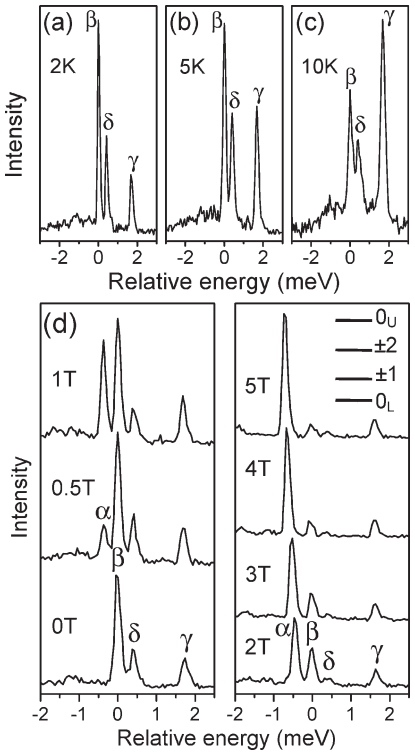

Figure 5. PL spectra of a single NC at various temperatures (2, 5, 10 K in (a), (b) and (c), respectively), and for various applied magnetic fields at 2 K (d). Each spectrum is recorded at an excitation intensity of 10 W/cm^2. The origin of the energy scale is 1.995 eV. The spectra display three ZPLs in zero field, labeled β, δ, and γ, while an extra line labeled α shows up under magnetic field. The emission lines α, β, δ, and γ are respectively attributed to the recombination ZPLs of the lowest fine structure states $|0_L\rangle$, $|\pm1\rangle$, $|\pm2\rangle$ and $|0_U\rangle$ in the crossover regime (see text).

luminescence of single NCs under steady-state excitation conditions. Figure 6a shows the pump intensity dependent PL spectrum of an individual NC at 2 K. The PL spectrum at 20 W/cm^2 displays a ZPL structure at ~1.96 eV (labeled X) attributed to the monoexciton states of a prolate NC. When rising the excitation intensity, an additional ZPL (labeled XX) ~12 meV red shifted with respect to the X structure shows up in the emission spectrum. As shown in Figure 6b, the integrated intensity of the X structure displays a linear growth with pump intensity, while that of the XX line has a quadratic dependence, which is clear evidence of its biexcitonic origin.

The shift of the biexciton recombination line with respect to the ground single exciton line provides a measure of the exciton−exciton interaction energy. A blue-shifted emission line attributed to biexciton recombination has been reported in single "giant" CdSe/CdS NCs, as a result of exciton−exciton repulsion.[31,32] Here, the red shift of the biexciton emission ZPL is indicative of an attractive exciton−exciton interaction in the CdSe core, which is in agreement with pionneering spectroscopic investigations led on NC ensembles at room temperature[24−30] and on single nanorods.[36] As shown in Figure 6c, the histogram of biexciton binding energies measured over 14 individual NCs is centered on ~12 meV, which is in accordance with the recent multiband calculations on spherical NCs.[37] Yet, calculations taking into account the shape dependence of the band-edge biexciton fine structure are still needed.

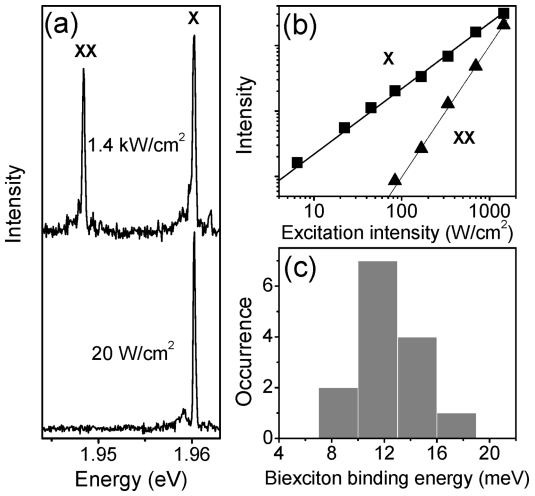

Figure 6. (a) PL spectra of a single NC at 2 K for two excitation intensities. X and XX label exciton and biexciton PL structures, respectively. (b) Integrated intensities of the X (squares) and XX (triangles) structures as a function of the pump intensity. (c) Distribution of the red shift of XX with respect to X for 14 individual NCs.

The biexciton radiative yield Q_{XX} is an important parameter for laser applications and for the generation of entangled photons.[38] We determined this parameter using two different approaches and found a large disparity (between 0.1 and unity). In the first method, cw laser excitation is used and Q_{XX} is extracted from the pump intensity dependence of the emission lines intensities. Figure 7(a) shows the PL spectra of a NC for which the XX peak becomes the dominant PL feature at high pump intensities (>200 W/cm^2). The integrated intensity of the XX structure displays a superlinear dependence on the excitation intensity, while that of the X shows a saturation behavior (see Figure 7(b)). Figure 7(c) also shows that the PL signal integrated over the entire emission spectrum scales linearly with the excitation intensity across the whole pump range studied in these measurements (0−3 kW/cm^2), even well above the onset for biexciton emission. This evolution is similar to that recently observed for "giant" CdSe/CdS single NCs.[31] The absence of saturation of the PL signal, together with the fact that the XX line largely prevails in the PL spectrum at high pump levels, indicate that the biexciton decay is primarily due to radiative recombination rather than Auger processes.

The biexciton quantum yield of the NC can be estimated from a simple three-level model of the luminescence signal which takes into account the zero-exciton ground level $|G\rangle$, a single exciton state $|X\rangle$ for simplicity, and the emitting biexciton state $|XX\rangle$ (see inset of Figure 7b). To derive the populations p_G, p_X, p_{XX} of these states, we consider a simple rate equation[39,40]

$$\begin{aligned} \dot{p}_G &= -Wp_G + \Gamma_X p_X \\ \dot{p}_X &= Wp_G + \Gamma_{XX}p_{XX} - (\Gamma_X + W)p_X \\ \dot{p}_{XX} &= Wp_X - \Gamma_{XX}p_{XX} \end{aligned}$$

where Γ_X and Γ_{XX} are the relaxation rates of the exciton and biexciton states, respectively, and W is the pumping rate from $|G\rangle$ to $|X\rangle$ and $|X\rangle$ to $|XX\rangle$. Assuming a purely radiative relaxation of $|X\rangle$,[12,41] the emission rates from $|X\rangle$ and from $|XX\rangle$ under cw laser excitation are given by $R_X = \Gamma_X p_X = (\Gamma_X\Gamma_{XX}W)/(\Gamma_X\Gamma_{XX} + \Gamma_{XX}W + W^2)$ and $R_{XX} = Q_{XX}\Gamma_{XX}p_{XX} = Q_{XX}(W/\Gamma_X)R_X$,

dx.doi.org/10.1021/nl202506c |Nano Lett. XXXX, XXX, 000–000

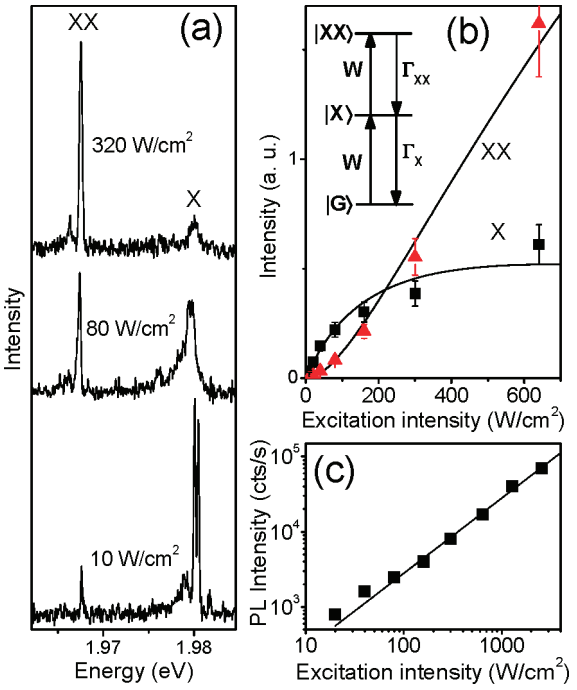

Figure 7. (a) PL spectra of a single NC at 2 K for various excitation intensities. X and XX label exciton and biexciton PL structures, respectively. (b) Integrated intensities of the X (squares) and XX (triangles) structures as a function of the pump intensity. The solid curves are the simulations derived from the three level model (ground, exciton, biexciton) depicted in inset and described in the text. They are plotted for $Q_{XX} = 1$ and $\Gamma_{XX}/\Gamma_X = 10$. (c) Evolution of the total PL intensity (measured with the avalanche photodiode) as a function of excitation intensity. The dashed line is a linear fit of this evolution.

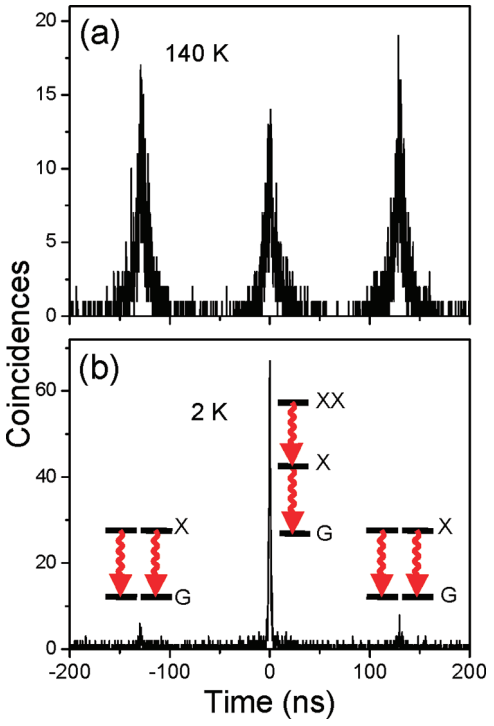

Figure 8. Photon coincidence histograms of a single NC under pulsed excitation with repetition period 130 ns, at 140 K (a) and at 2 K (b). The mean number of exciton created per pulse is 0.2. The time resolution is 152 ps. In the high temperature regime (a), the 7 ns characteristic decay time corresponds to the exciton lifetime. The area ratio of the central peak to a lateral peak is 0.8 and provides a direct determination of the biexciton to exciton quantum yield ratio. At 2 K, exciton shelving in this long-lived state results in a pronounced photon bunching.

respectively. These expressions reproduce well both experimental evolutions of the integrated X and XX intensities in Figure 7b with a common laser intensity scaling factor and a common detection yield scaling factor. It is important to note that the relative evolution of R_X and R_{XX} critically depends on Q_{XX}, and only values $Q_{XX} \sim 1$ well reproduce the data when $\Gamma_{XX}/\Gamma_X \geq 10$. Such a ratio is realistic considering the orders of magnitudes found in the literature for the biexciton radiative lifetime (~10 ns[42]), as well as the mean exciton lifetime 160 ns of this NC at low temperatures.[43] The high value found for Q_{XX} contrasts with those previously reported for CdSe NCs ($Q_{XX} \sim 0.1$)[39,42] and points to a strong dependence of Q_{XX} on the NC geometry. It turns out that all single NCs whose spectroscopic signatures are in the spherelike regime of Figure 1d do not show the spectral signature of a radiative biexciton recombination. These observations support the idea that Auger recombination processes can be greatly reduced in relatively large and elongated NCs.[19,44]

The second method employed to determine Q_{XX} relies on the study of the PL intensity $I(t)$ autocorrelation function,[32,39] $g^{(2)}(\tau) = \langle I(t)I(t+\tau)\rangle/\langle I(t)\rangle^2$. Figure 8 exemplifies the temperature evolution of the photon coincidence histograms for a single NC under a weak pulsed excitation leading to the creation of a mean number of 0.2 exciton per pulse. As expected, the coincidence histograms consist of a series of discrete peaks occurring at whole numbers of the laser period (130 ns). While the lateral peaks are due to coincidences between photons stemming from different PL bursts, the weight of the central peak reflects the probability that two photons were emitted within a single PL burst. For instance, the central peak would be identical in intensity and shape to the lateral ones for the Poissonian light states of a pulsed periodic coherent source (such as an attenuated laser[45,46]), but it should vanish altogether if only a single photon was emitted in each PL burst. Therefore, the intensity ratio of the central peak to lateral ones is directly related to the fraction of PL bursts giving two or more photons. At room temperature and in the limit of low pump intensities, this ratio tends to Q_{XX}/Q_X, where Q_X is the exciton radiative yield.[39] Assuming $Q_X = 1$,[12,41] we deduce $Q_{XX} = 0.8$ from the correlation histogram recorded at 140 K (see Figure 8a), where fine structure states are thermally mixed. The analysis of the PL photon statistics therefore confirms the finding of high biexciton quantum yields evidenced in the PL spectra.

The weak photon antibunching observed in the high-temperature regime turns to a striking photon bunching at 2 K, as shown in Figure 8b. This observation points to the shelving role played by the dark ground excitonic state when its lifetime is comparable to the laser repetition period. All investigated NCs displayed this behavior, as expected given that the ground excitonic state is long-lived in spherelike, crossover, or rodlike NC fine structures.

In conclusion, magneto-optical studies of highly photostable single CdSe/ZnS NCs with a large distribution of shapes unveiled a variety of band-edge exciton fine structures that are consistent with the existing theoretical models. A deeper understanding of the shape dependent band-edge exciton fine

dx.doi.org/10.1021/nl202506c |Nano Lett. XXXX, XXX, 000–000

structures will require the development of a correlative microscopy of the geometry and the spectroscopic properties of single NCs. An important finding of the present study is the signature of a highly efficient biexciton radiative recombination in the low-temperature PL spectra and PL intensity autocorrelation function of single NCs. An explanation for the large disparity of biexciton radiative yields (between 0.1 and 1) requires the elaboration of theoretical models that take into account the shape dependence of the biexciton fine structure and the Auger rates. Besides its fundamental interest, the determination of the NC geometry that maximizes the biexciton quantum yield is crucial in the view of applications in quantum information processing and laser technologies.

AUTHOR INFORMATION

Corresponding Author
*E-mail: blounis@u-bordeaux1.fr.

ACKNOWLEDGMENT

We thank Satyabrata Si and Marie-Hélène Delville for TEM measurements. This work was funded by the Agence Nationale de la Recherche, Région Aquitaine, the French Ministry of Education and Research, and the European Research Council.

REFERENCES

(1) Zutic, I.; Fabian, J.; Das Sarma, S. *Rev. Mod. Phys.* **2004**, *76* (2), 323–410.
(2) Loss, D.; DiVincenzo, D. P. *Phys. Rev. A* **1998**, *57* (1), 120–126.
(3) Colvin, V. L.; Schlamp, M. C.; Alivisatos, A. P. *Nature* **1994**, *370* (6488), 354–357.
(4) Dabbousi, B. O.; Bawendi, M. G.; Onitsuka, O.; Rubner, M. F. *Appl. Phys. Lett.* **1995**, *66* (11), 1316–1318.
(5) Schlamp, M. C.; Peng, X. G.; Alivisatos, A. P. *J. Appl. Phys.* **1997**, *82* (11), 5837–5842.
(6) Coe, S.; Woo, W. K.; Bawendi, M.; Bulovic, V. *Nature* **2002**, *420* (6917), 800–803.
(7) Bruchez, M.; Moronne, M.; Gin, P.; Weiss, S.; Alivisatos, A. P. *Science* **1998**, *281* (5385), 2013–2016.
(8) Michalet, X.; Pinaud, F. F.; Bentolila, L. A.; Tsay, J. M.; Doose, S.; Li, J. J.; Sundaresan, G.; Wu, A. M.; Gambhir, S. S.; Weiss, S. *Science* **2005**, *307* (5709), 538–544.
(9) Nirmal, M.; Norris, D. J.; Kuno, M.; Bawendi, M. G.; Efros, A. L.; Rosen, M. *Phys. Rev. Lett.* **1995**, *75* (20), 3728–3731.
(10) Efros, A. L.; Rosen, M.; Kuno, M.; Nirmal, M.; Norris, D. J.; Bawendi, M. *Phys. Rev. B* **1996**, *54* (7), 4843–4856.
(11) Klimov, V. I. *Semiconductor and Metal Nanocrystals:Synthesis and Electronic and Optical Properties*; Marcel Dekker, Inc.: New York, 2004.
(12) Labeau, O.; Tamarat, P.; Lounis, B. *Phys. Rev. Lett.* **2003**, *90* (25), 257404.
(13) Biadala, L.; Louyer, Y.; Tamarat, P.; Lounis, B. *Phys. Rev. Lett.* **2009**, *103* (3), 037404.
(14) Louyer, Y.; Biadala, L.; Tamarat, P.; Lounis, B. *Appl. Phys. Lett.* **2010**, *96* (20), 203111.
(15) Fernee, M. J.; Littleton, B. N.; Rubinsztein-Dunlop, H. *ACS Nano* **2009**, *3* (11), 3762–3768.
(16) Biadala, L.; Louyer, Y.; Tamarat, P.; Lounis, B. *Phys. Rev. Lett.* **2010**, *105* (15), 157402.
(17) Peng, X. G.; Manna, L.; Yang, W. D.; Wickham, J.; Scher, E.; Kadavanich, A.; Alivisatos, A. P. *Nature* **2000**, *404* (6773), 59–61.
(18) Hu, J. T.; Li, L. S.; Yang, W. D.; Manna, L.; Wang, L. W.; Alivisatos, A. P. *Science* **2001**, *292* (5524), 2060–2063.
(19) Htoon, H.; Hollingsworth, J. A.; Dickerson, R.; Klimov, V. I. *Phys. Rev. Lett.* **2003**, *91* (22), 227401.
(20) Shabaev, A.; Efros, A. L. *Nano Lett.* **2004**, *4* (10), 1821–1825.
(21) Le Thomas, N.; Herz, E.; Schops, O.; Woggon, U.; Artemyev, M. V. *Phys. Rev. Lett.* **2005**, *94* (1), 016803.
(22) Klimov, V. I.; Mikhailovsky, A. A.; Xu, S.; Malko, A.; Hollingsworth, J. A.; Leatherdale, C. A.; Eisler, H. J.; Bawendi, M. G. *Science* **2000**, *290* (5490), 314–317.
(23) Klimov, V. I.; Mikhailovsky, A. A.; McBranch, D. W.; Leatherdale, C. A.; Bawendi, M. G. *Science* **2000**, *287* (5455), 1011–1013.
(24) Klimov, V.; Hunsche, S.; Kurz, H. *Phys. Rev. B* **1994**, *50* (11), 8110–8113.
(25) Sewall, S. L.; Cooney, R. R.; Anderson, K. E. H.; Dias, E. A.; Kambhampati, P. *Phys. Rev. B* **2006**, *74* (23), 235328.
(26) Sewall, S. L.; Cooney, R. R.; Anderson, K. E. H.; Dias, E. A.; Sagar, D. M.; Kambhampati, P. *J. Chem. Phys.* **2008**, *129* (8), 084701.
(27) Achermann, M.; Hollingsworth, J. A.; Klimov, V. I. *Phys. Rev. B* **2003**, *68* (24), 245302.
(28) Caruge, J. M.; Chan, Y. T.; Sundar, V.; Eisler, H. J.; Bawendi, M. G. *Phys. Rev. B* **2004**, *70* (8), 085316.
(29) Bonati, C.; Mohamed, M. B.; Tonti, D.; Zgrablic, G.; Haacke, S.; van Mourik, F.; Chergui, M. *Phys. Rev. B* **2005**, *71* (20), 205317.
(30) Sewall, S. L.; Franceschetti, A.; Cooney, R. R.; Zunger, A.; Kambhampati, P. *Phys. Rev. B* **2009**, *80* (8), 081310(R).
(31) Htoon, H.; Malko, A. V.; Bussian, D.; Vela, J.; Chen, Y.; Hollingsworth, J. A.; Klimov, V. I. *Nano Lett.* **2010**, *10* (7), 2401–2407.
(32) Park, Y. S.; Malko, A. V.; Vela, J.; Chen, Y.; Ghosh, Y.; Garcia-Santamaria, F.; Hollingsworth, J. A.; Klimov, V. I.; Htoon, H. *Phys. Rev. Lett.* **2011**, *106* (18), 187401.
(33) Osovsky, R.; Cheskis, D.; Kloper, V.; Sashchiuk, A.; Kroner, M.; Lifshitz, E. *Phys. Rev. Lett.* **2009**, *102* (19), 197401.
(34) Zhang, K.; Chang, H. Y.; Fu, A. H.; Alivisatos, A. P.; Yang, H. *Nano Lett.* **2006**, *6* (4), 843–847.
(35) Zhao, Q.; Graf, P. A.; Jones, W. B.; Franceschetti, A.; Li, J.; Wang, L. W.; Kim, K. *Nano Lett.* **2007**, *7* (11), 3274–3280.
(36) Le Thomas, N.; Allione, M.; Fedutik, Y.; Woggon, U.; Artemyev, M. V.; Ustinovich, E. A. *Appl. Phys. Lett.* **2006**, *89* (26), 263115.
(37) Rodina, A. V.; Efros, A. L. *Phys. Rev. B* **2010**, *82* (12), 125324.
(38) Stevenson, R. M.; Young, R. J.; Atkinson, P.; Cooper, K.; Ritchie, D. A.; Shields, A. J. *Nature* **2006**, *439* (7073), 179–182.
(39) Nair, G.; Zhao, J.; Bawendi, M. G. *Nano Lett.* **2011**, *11* (3), 1136–1140.
(40) In this simple model, we neglect the triexciton population because we assume that the triexciton recombination is much faster than the relaxation dynamics of the mono- and biexcitons.
(41) Brokmann, X.; Coolen, L.; Dahan, M.; Hermier, J. P. *Phys. Rev. Lett.* **2004**, *93* (10), 107403.
(42) Fisher, B.; Caruge, J. M.; Zehnder, D.; Bawendi, M. *Phys. Rev. Lett.* **2005**, *94* (8), 087401.
(43) The PL decay at low pump levels is triexponential with characteristic times 1.1, 14.3, and 233 ns, which have relative intensity weights 14, 19, and 67%, respectively.
(44) Cragg, G. E.; Efros, A. L. *Nano Lett.* **2010**, *10* (1), 313–317.
(45) Brunel, C.; Lounis, B.; Tamarat, P.; Orrit, M. *Phys. Rev. Lett.* **1999**, *83* (14), 2722–2725.
(46) Lounis, B.; Moerner, W. E. *Nature* **2000**, *407* (6803), 491–493.